

WIND TUNNEL TESTING OF A 6%-SCALE LARGE CIVIL TILT ROTOR MODEL IN AIRPLANE AND HELICOPTER MODES

Colin R. Theodore
Gina C. Willink
Carl R. Russell
Aeromechanics Office
NASA Ames Research Center
Moffett Field, CA

Alexander R. Amy
Monterey Technologies, Inc.
NASA Ames Research Center
Moffett Field, CA

Ashley E. Pete
Aviation Development Directorate-AFDD (AMRDEC)
U.S. Army Research, Development and Engineering
Command
Ames Research Center
Moffett Field, CA

In April 2012 and October 2013, NASA and the U.S. Army jointly conducted a wind tunnel test program examining two notional large tilt rotor designs: NASA's Large Civil Tilt Rotor and the Army's High Efficiency Tilt Rotor. The approximately 6%-scale airframe models (unpowered) were tested without rotors in the U.S. Army 7- by 10-foot wind tunnel at NASA Ames Research Center. Measurements of all six forces and moments acting on the airframe were taken using the wind tunnel scale system. In addition to force and moment measurements, flow visualization using tufts, infrared thermography and oil flow were used to identify flow trajectories, boundary layer transition and areas of flow separation. The purpose of this test was to collect data for the validation of computational fluid dynamics tools, for the development of flight dynamics simulation models, and to validate performance predictions made during conceptual design. This paper focuses on the results for the Large Civil Tilt Rotor model in an airplane mode configuration up to 200 knots of wind tunnel speed. Results are presented with the full airframe model with various wing tip and nacelle configurations, and for a wing-only case also with various wing tip and nacelle configurations. Key results show that the addition of a wing extension outboard of the nacelles produces a significant increase in the lift-to-drag ratio, and interestingly decreases the drag compared to the case where the wing extension is not present. The drag decrease is likely due to complex aerodynamic interactions between the nacelle and wing extension that results in a significant drag benefit.

Notation

C_D	Drag coefficient, non-dimensional
C_L	Lift coefficient, non-dimensional
D	Drag, lb
L	Lift, lb
L/D	Lift/Drag, non-dimensional
q	Dynamic pressure, lb/ft-s ²
Re	Reynolds number, non-dimensional
V	Flow velocity, knots
α	Angle of attack, deg
β	Angle of sideslip, deg

Introduction

In April 2012 and October 2013, NASA and the U.S. Army jointly conducted a wind tunnel test program examining two notional large tilt rotor designs: NASA's Large Civil Tilt Rotor (LCTR) and the Army's High

Efficiency Tilt Rotor (HETR). The approximately 6% scale airframe models were tested without rotors in the U.S. Army 7- by 10-foot wind tunnel at NASA Ames Research Center. This test entry represents the first wind tunnel data for the LCTR configuration as shown in Figure 1. This paper focuses on the results for the LCTR model in airplane mode at high speed. Data were also collected at low speed in a helicopter mode configuration, however these data are not included in this paper.

The similarities between the LCTR and HETR aircraft allowed a significant amount of hardware to be shared between the two models, which reduced fabrication, build-up and model reconfiguration time, and ultimately reduced the cost of the test entry. In particular, the HETR wing and nacelle geometries were incorporated into the LCTR wind tunnel model. Therefore the LCTR wind tunnel model and the LCTR design of Ref. 1 are not entirely consistent.

The purpose of this test was to collect data for the validation of computational fluid dynamics tools, for the development of flight dynamics simulation models, and to validate and refine performance predictions made during conceptual design. This test also provides insights into the aerodynamic performance of the LCTR configuration, and the contribution of the various aerodynamic components to the overall aerodynamics, in particular the wing, nacelles and wing extensions.

Recent studies of the hover and low-speed flight control and handling qualities aspects of the LCTR configuration have been reported in Refs. 2-5. The flight dynamics models used for these studies were based on state-space linear models generated from CAMRAD II (Ref. 6) and used a simple linear representation of fuselage and airframe aerodynamics as functions of the body velocity components. The LCTR data from this wind tunnel test, along with rotor interaction effects calculated using RotCFD (Ref. 7), will be used to refine the aerodynamics of the vehicle in hover and low speed flight, particularly in sideward, rearward, and ascending and descending flight with angles of attack and sideslip beyond the linear aerodynamic range.

A similar investigation was recently conducted by AugustaWestland and Politecnico di Milano on a 1:8 scale model of the Enhanced Rotorcraft Innovative Concept Achievement (ERICA) tilt rotor design (Ref. 8). That wind tunnel test examined the aerodynamic forces and moments of several different configurations of the ERICA model and at different attitudes, including some conditions at very high incidences and sideslip angles. Reference 8 shows the drag contributions of the various airframe components, including the fuselage, wing, wing fairing, sponsons, nacelles, fin and horizontal tailplane, however the ERICA model did not include wing extensions.

The current paper describes the experimental setup, including the wind tunnel, baseline LCTR model, and various derivative configurations. Next, the test matrix is described. Results are presented for the high-speed portion of the test matrix, including testing with the full LCTR model with various wing tip configurations, and wing-only testing with various tip configurations. Finally, the conclusions of this work are presented, as well as suggestions for follow-on wind tunnel testing and data analysis.

Experimental Setup

Wind Tunnel

The wind tunnel test was conducted in the U.S. Army 7-

by 10-foot wind tunnel at NASA Ames Research Center. The tunnel is a closed return wind tunnel with a maximum flow speed of 220 knots or a Mach number of 0.3. The wind tunnel is equipped with a turntable mounted on a scale-system that was used to measure the aerodynamic loads presented in this paper. The model was installed on a three-point mounting system in the wind tunnel, with two forward struts connected to the wing slightly inboard of the nacelle location. An aft strut was connected to the tail of the airframe. Pitching of the model was achieved by extending and retracting the tail strut to allow for a model pitch range of -10 to +12 deg. The turntable provided -180 to +180 degrees of model sideslip. The mounting system is shown in Figure 2. Figure 2 also shows a set of circular fairings on the forward struts that were used for the low-speed cases. These fairings allowed the model to be tested at +/- 180 degrees of yaw, which was required for the low-speed portions of the test matrix that included nacelle helicopter and transition configurations.

The LCTR model in airplane mode is shown in Figure 3. Figure 3 also shows the aerodynamic fairings that were installed over the two forward struts and tail strut for high-speed testing that reduced the aerodynamic effects of the strut fairings on the model and also reduced the amount of blockage caused by the model support system. The wind tunnel does not have automatic counter-rotating strut fairings that keep the fairings aligned with the freestream as the turntable rotates. For this reason, during high-speed testing, each time a new sideslip angle was tested, the aerodynamic fairings had to be rotated manually from within the test section. This mounting configuration also allowed for wing-only testing in which case, the tail strut was removed, as shown in Figure 4.

The aerodynamic forces and moments on the model were measured using the wind tunnel scale system. Table 1 shows the measurement range and accuracy of this scale system. The lift force is measured to an accuracy of about 1-2 lb, while the drag force is measured to an accuracy of about 0.5 lb.

Model Description

The similarities between the LCTR and HETR aircraft allowed a significant amount of hardware to be shared between the two models, which reduced fabrication, build-up and model reconfiguration time, and ultimately reduced the cost of the test entry. The models shared a common wing and nacelles components that were scaled from the HETR geometry. The individual fuselage and tail sections were both mounted on a common strongback that consisted of a 4-inch square aluminum tube that runs down the center of the fuselage. The outer fuselages for the LCTR and HETR consisted of panels that were

manufactured using a Selective Laser Sintering (SLS) technique and Nylon 12 GF, which is a glass-filled nylon material. Sets of ribs were used to attach the SLS fuselage panels to the fuselage strongback. Figure 5 shows examples of the aluminum ribs and SLS fuselage panels, and the build-up of the LCTR model in the wind tunnel. Different sets of ribs and fuselage panels were used for the LCTR and HETR models because of the different fuselage profiles and diameters of the two aircraft. The wing and LCTR tail section were machined from aluminum.

The nacelles and wing extensions were manufactured using SLS and the same material as the fuselage panels. The nacelles were made in two halves with an aluminum plate located at the vertical center of the nacelle. This plate provided an anchor to attach the wing extensions to the nacelles. The connection between the wing and nacelles enabled the nacelle angle to be set independently of the wing. High-speed testing with a nacelle incidence of zero degrees, as well as low-speed testing with angles from 60 degrees (30 degrees forward of vertical) to 95 degrees (5 degrees aft of vertical) was possible.

Table 2 compares the full-scale LCTR geometry with the LCTR wind tunnel model as tested. The wind tunnel model was 6% full-scale. As previously mentioned, the LCTR wind tunnel model uses the wing and nacelle configuration and geometry from the HETR design. The HETR wing uses the 21% thick airfoil section that was developed under an U.S. Army SBIR contract[†]. This HETR airfoil section is specifically designed to maintain natural laminar flow on a tilt rotor wing in cruise. A thick airfoil is necessary on a tilt rotor for high-flapping stiffness for whirl flutter stability, and the need to house a cross-shaft between the nacelles.

Figure 6 shows the wing and fuselage pitch angle definitions relative to the wind tunnel freestream flow. A notional NACA4421 airfoil (21% maximum thickness) is shown in Figure 6 for illustrative purposes only and does not represent the actual HETR airfoil geometry. The angle of attack of the fuselage is referenced to the waterline of the fuselage (Fuselage Reference Line in Fig. 6), and this waterline is parallel to the freestream at zero angle of attack. The wing incidence is referenced to the airfoil chordline, and the incidence is +3.3 deg relative to the fuselage reference line, also shown as shown in Figure 6. For consistency, all plots in this report are plotted using the fuselage waterline as a reference in measuring angle of attack. For wing-only testing, the wing is at an

[†] The airfoil section geometry developed under a U.S. Army SBIR contract for the HETR design is proprietary and cannot be shown in this paper.

incidence of +3.3 degrees for a zero angle of attack. This will be discussed further in the results section.

Figure 7 shows a graphic and photos of the three different wing-tip configurations tested. The first configuration was with a wing cap installed and the nacelle and wing tip removed. The wing cap geometry is shown with the red solid lines in Figure 7, and extends to the mid point of where the nacelle would be installed. The outboard end of the wing cap is not rounded, but rather a squared-off wing tip is used. The second configuration is with the wing cap removed and the nacelle installed. With reference to Figure 7, this configuration is without the yellow wing extension installed. The third configuration is with the wing extension with squared-off tip installed on the nacelle.

Test Matrix

The test matrix for the LCTR model included high-speed testing (up to 200 knots) in an airplane mode configuration with the engine nacelles parallel to the flow and low-speed testing (up to 80 knots) with nacelle in helicopter and transition configurations.

Low-Speed Testing

The LCTR low-speed testing was performed mostly for validation of computational fluid dynamics tools and for the development of flight dynamics simulation models. The model was configured in helicopter and transition modes with the nacelles tilted at various angles between 60 and 95 deg, where 90 deg is helicopter mode, and 0 deg is airplane mode. Figure 8 shows a photo of the LCTR in the helicopter-mode configuration with the nacelles at 90 deg. This figure also shows an example of oil flow imagery used to qualitatively assess flow characteristics on each component. The sideslip, or yaw angle, was varied from -180 to +180 deg simulating low-speed flight in any direction, including sideward and aft flight. The fuselage pitch angle ranged between -10 and +12 deg.

High-Speed Testing

The LCTR high-speed test data was acquired primarily for validating computational fluid dynamics predictions, and to validate performance predictions made during conceptual design. Testing was performed in airplane mode with the nacelles parallel to the flow at speeds of up to 200 knots. The angles of attack and sideslip ranged between -10 and +12 deg. High-speed testing was also performed with the wing-only (no fuselage or tail) and the various nacelle and wing extension combinations.

Results

Results from the high-speed portion of this test are reported in this paper. The wind tunnel experiment consisted of a total of 556 data runs including weight tare and aero tare runs, as well as research data collection runs. The data presented represent mean values computed from 2500 samples recorded at 100 Hz over 25 seconds.

A series of runs were conducted to examine the effect of Reynolds number on the measurements. Figure 9 shows the lift and drag coefficients for Reynolds numbers of approximately 0.8×10^6 , 1.2×10^6 , and 1.4×10^6 for the LCTR airframe model with the nacelles and wing extensions included for $\beta=0$ deg. A Reynolds number of 1.2×10^6 corresponds to $V = 168$ knots and a dynamic pressure, q , of 94 lb/ft^2 , where these quantities vary slightly with the air density and temperature for a given Reynolds number. Trip dots were placed along the span of the wing at the 55% chord location to ensure flow transition at a point consistent with the design of the airfoil section. Trip dots were also placed on the nacelles at about 5% from the nacelle leading edge at approximately the aft end of the rotor spinner. Trip dots were also attached to the fuselage, aft of the nose at the point where the constant diameter of the fuselage begins; slightly forward of the wing; and along the span of the V-tail at a 5% chord location. These trip dot locations were consistent throughout the high-speed portion of the wind tunnel test, including during wing-only testing.

Figure 9 shows that there is essentially no effect of Reynolds number on the lift coefficient. The drag coefficient shows a slight increase with Reynolds number at high angles of attack to a maximum increase of about 10% from Reynolds number of 0.8×10^6 to 1.4×10^6 at an angle of attack of +12 deg. However there is only a very small effect of Reynolds number in the region from -5 to +5 deg, which is the primary alpha range for this experiment. Since the effects of Reynolds number are small, the remainder of the results presented in this paper is for a Reynolds number of 1.2×10^6 .

Figure 10 shows the effects of the different wing tip configurations on the L/D, Lift/q and Drag/q values for the airframe at a sideslip angle of zero. The dimensional quantities of lift and drag are normalized by the dynamic pressure (q) to remove the effects of the slight differences in wind tunnel speeds in the different sets of data. Looking first at Figure 10(a), the L/D plots show that the addition of the nacelle results in a slight decrease in the L/D. The further addition of the wing extension produces a significant increase in L/D with a peak at about 16 at an angle of attack of 2 deg as compared with a maximum L/D of 12 for the case without the wing extension. The slope of the L/D curve increases with the addition of the

wing extensions due to the additional wing area producing more lift for each increment in angle of attack.

Figure 10(b) shows the Lift/q for the LCTR model with the three different wing-tip configurations. The addition of the nacelle to the wing increases the amount of lift generated, particularly at higher angles of attack. In this case, the nacelle acts as a pseudo flat-plate at the end of the wing that results in a more 2-D wing lift distribution, increasing the amount of the lift that the wing produces. The nacelle also contributes to some of the lift increase. The wing tip configuration with the wing cap has a squared-off wing tip and is not aerodynamically optimized. This would result in a decrease in lift and an increase in drag when compared with a similar wing with an aerodynamically optimized wing tip. The addition of the wing extension to the nacelle produces a significant increase in L/D and also an increase in the slope of the lift versus alpha curve.

The model angle of attack for zero lift is about -6.0 deg and is fairly independent of the wing tip configuration. At -6.0 deg, the wing is at an incidence of about -2.7 deg relative to the flow since the wing is inclined at +3.3 deg relative to the fuselage. Since the wing airfoil is highly cambered, positive lift is still produced at -2.7 deg. This wing lift balances out the negative lift generated by the fuselage and tail at -6.0 deg.

Figure 10(c) shows the Drag/q for the LCTR model with the three different wing tip configurations. The addition of the nacelle adds a fairly constant increment in drag over the angle of attack range tested. When the wing extension is added, the drag actually decreases compared to the nacelle-alone case. The drag with the wing extension is similar to the level with the wing cap only from about 2-5 deg of angle of attack. At either end of the angle of attack spectrum, the drag with wing extension increases to the drag level with nacelle only.

The drag results of Fig. 10(c) are somewhat counter intuitive since adding an additional lifting surface outboard of the nacelle is expected to increase the total airframe drag, particularly given the large increase in lift (and subsequent induced drag) that the addition of the wing extension produces. However, Fig. 10(c) shows that there is essentially no increase in drag with the addition of the wing extension compared to the case with the nacelle alone at any of the angles of attack tested. Since this result is somewhat unexpected, an investigation was conducted to determine if measurement errors or other interactions results in a decrease in drag with the addition of the wing extensions.

The model changes between the different wing-tip configurations are only to the outboard portion of the

wing, and therefore different interactions of the wing-tip wake on the fuselage or tail with the addition of the nacelle and wing extension is unlikely. It is also unlikely that the changes in the wing-tip configuration altered the aerodynamic interactions between the model and support structure since the forward struts are connected inboard of the nacelles and the tail strut is at the centerline of the model behind the fuselage and tail. The processing of the data for weight tares affects only the pitching and rolling moment measurements, so weight tare corrections do not contribute to changes in drag measurements. The aerotare corrections for each of these measurements are based on the angle of attack and dynamic pressure. Since the angle of attack and dynamic pressure are essentially the same for each model configuration tested, the aerotare corrections are also basically the same for each set of data.

Figures 11 and 12 show the same data as shown in Figure 10, but at sideslip angles of +5.0 and +10.0 deg, respectively, compared to a sideslip angle of 0 deg for Figure 10. The data in Figure 11 for a sideslip angle of +5.0 deg shows a similar trend as seen in Figure 10 where the addition of the nacelle produces an almost uniform increase in drag with angle of attack. Figure 11 also shows that the drag decreases with the addition of the wing extension, although by a reduced amount when compared with the zero sideslip data, and over a reduced angle of attack range. Examination of Figure 12 at a sideslip angle of +10.0 deg shows that the addition of the wing extension still produces a significant increase in L/D and overall lift, but the drag benefits seen at smaller sideslip angles are no longer present. Therefore, the drag reductions with the wing extension are sensitive to the sideslip angle and disappear at a sideslip angle of about +10.0 deg.

The data shown in Figures 10-12 were collected first at a sideslip angle of 0 deg for each model configuration, then at a sideslip angle of +5.0 deg for each model configuration, and finally at a sideslip angle of +10.0 deg for each model configuration. Since the drag trends are similar for the different sideslip angle cases, an issue with the wing tunnel scale measurement system would not contribute to the drag differences seen in Figures 10-12.

A likely explanation for the drag trends seen in Figures 10 and 11 is that there is a complex beneficial aerodynamic interaction in the region of the nacelle and wing extension interface that produce a reduction in drag. Without a wing extension, there is a complex 3-D flow around the nacelle that is no longer present when the wing extension is attached. The nacelle acts more as a 2-D object since the wing extension prevents the flow from wrapping or rolling around the nacelle. A number of oil flow runs were performed during the wind tunnel entry, however

none of these examined the flow around the nacelles with and without the wing extensions. Examination of the flow around the nacelle and wing extension would be an important part of a follow-on test entry.

A final set of results is presented in Figure 13 for the wing-only model configurations shown in Figure 4. Figure 13 shows the L/D, Lift/q and Drag/q at a Reynolds number of 1.2×10^6 and at $\beta=0$ deg. Since there was no tail strut to change the model pitch angle, the wing angle of attack was set by inserting a set-screw in the connection between the forward struts and the wing, so precisely setting the wing angle was difficult. The uncertainty in the angle of attack measurement is approximately 0.2 – 0.3 deg in the data shown in Figure 13. As shown in Table 1, the accuracy of the drag measurement is about +/- 0.5 lb. The drag measurements shown in Figure 13(c) are as low as Drag/q of 0.1, which is about 9.0 lb of drag. Therefore, the uncertainty in the drag measurement may be of the order of +/- 5-10%.

Figure 13(a) shows that the maximum L/D of about 22 is measured with the configuration with the wing, nacelle and wing extension, as compared to an L/D of about 16 with the wing extension removed. The Lift/q plot shows that there is only a slight increase in lift with the addition of the nacelle, but a much larger increase with the further addition of the wing extension. Figure 13(b) also shows that the zero lift line for the wing is approximately -8 to -9 deg angle of attack. Recall that the definition of the wing angle of attack is consistent with that of the fuselage such that a zero angle of attack corresponds to a +3.3 deg wing incidence. When this +3.3 deg incidence is accounted for, the angle attack for zero lift would be of the order of -5 to -6 deg. This is consistent with the zero lift angle of attack of the Clark Y airfoil that has similar camber and a zero lift angle of attack of about -5 deg.

Figure 13(c) shows the Drag/q measurement for the wing with different wing tip configurations. These data show that the addition of the wing extension reduces the overall drag compared to the case with the nacelle alone. The reduction in Drag/q measurement is of the order of 0.01-0.02 (or about 1-2 lb), which is consistent with the drag reduction shown in Figure 10 at similar angles of attack, and confirms the aerodynamic benefits achieved with the addition of the wing extension. Future work, both experimental and analytical, should focus on whether the drag benefits are retained with rotors present.

Summary and Conclusions

A 6%-scale model of the Large Civil Tilt Rotor (LCTR) concept was tested in the U.S. Army 7- by 10-foot wind tunnel at NASA Ames Research Center. The model was unpowered and tested without rotors. The purpose of this

test was to collect data for the validation of computational fluid dynamics tools, for the development of flight dynamics simulation models, and to validate performance predictions made during conceptual design. These data represent the first aerodynamic measurements of the LCTR configuration. This paper focuses on the results for the LCTR model in an airplane-mode configuration up to 200 knots. Measurements were taken of the aerodynamic forces and moments using the wind tunnel scale system, and data is presented for the full LCTR model with various wing tip configurations for variations in speed, angle of attack from -10 to +12 deg, and sideslip angles from 0 to +10 deg. Measurements of an isolated wing with various wing-tip configurations were also acquired.

The following conclusions can be drawn from this experiment:

- 1) The addition of the nacelle to the LCTR wing produces an increase in lift due to the nacelle acting as a pseudo flat plate at the end of the wing that produces a more rectangular lift distribution, however the increase in drag associated with the nacelle decreases the L/D of the airframe due to the larger increase in drag.
- 2) The further addition of the wing extension produces a significant increase in lift and L/D when compared with a configuration with a nacelle, but without a wing extension. The L/D increases from about 12 to 16 as a result of the addition of the wing extension outboard of the nacelle.
- 3) The addition of the wing extension to the nacelle decreases the overall drag of the model, particularly in the angle of attack region of maximum L/D at about 2 deg nose-up attitude. This result is confirmed when looking at data for the wing-only configuration. There appears to be a complex beneficial aerodynamic interaction between the nacelle and wing extension that results in a decrease in drag when the wing extension is added. The wind tunnel data show that this drag benefit is sensitive to sideslip angle and is less as sideslip increases, and disappears at a sideslip angle of about +10 deg.

Future Work

Initial CFD comparisons with the wind tunnel data are being performed with the RotCFD mid-fidelity computational fluid dynamics tool (Ref. 7) that was developed by Sukra Helitech, Inc. specifically to aid in rotorcraft conceptual design efforts. The key components of RotCFD are a geometry module, a grid generation module, a Navier-Stokes flow-solver module, a blade

element rotor model, and flow visualization and analysis modules. The goal of analyzing the wind tunnel model using RotCFD is first to validate the bare-airframe (no rotors) aerodynamic predictions against the measurements made in the wind tunnel for the LCTR model. Once an airframe aerodynamic model has been validated, a rotor model will be added to the analysis to predict the aerodynamic interactions between the rotor wake and the airframe to enable performance and loads predictions with rotor interactions. These predictions will allow for more accurate tilt rotor performance prediction at the vehicle conceptual design level. RotCFD was recently used in a study of tilt rotor wake interactions resulting from operations near vertiport terminals (Ref. 9). This work used RotCFD to analyze the level of interactions between the rotor wake and ground infrastructure such as terminal buildings and jetways in order to perform an assessment of the impacts and ultimately develop concepts of operations for large tilt rotor aircraft around airport infrastructure.

A follow-on wind tunnel test of the LCTR configuration is recommended, in addition to the CFD analysis and validation activities. This follow-on test would add rotors to the model and perform a powered test of the full LCTR configuration to determine the effectiveness of the wing laminar flow airfoil used, and further examine the aerodynamic interactions, in particular between the nacelle and wing extension in the presence of a rotor wake.

References

1. Acree, Jr., C. W., Yeo, H., and Sinsay, J. D., "Performance Optimization of the NASA Large Tiltrotor," NASA/TM-2008-215359, June 2008.
2. Blanken, C. L., Lusardi, J. A., Ivler, C. M., Tischler, M. B., Decker, W. A., Malpica, C. A., Berger, T., and Tucker, G. E., and Höfingler, M. T., "An Investigation of Rotorcraft Stability – Phase Margin Requirements in Hover," American Helicopter Society 65th Annual Forum, Grapevine, TX, May 27-29, 2009.
3. Malpica, C. A., Decker, W. A., Theodore, C. R., Blanken, C. L., and Berger, T., "An Investigation of Large Tilt-Rotor Short-term Attitude Response Handling Qualities Requirements in Hover." American Helicopter Society 66th Annual Forum, Phoenix, AZ, May 11-13, 2010.
4. Malpica, C. A., Decker, W. A., Theodore, C. R., Lawrence B., Lindsey, J., and Blanken, C. L., "An Investigation of Large Tilt-Rotor Hover and Low Speed Handling Qualities Requirements," American Helicopter

Society 67th Annual Forum, Virginia Beach, VA, May 3-5, 2011.

5. Malpica, C. A., Theodore, C. R., Lawrence, B., Blanken, C. L., and Lindsey, J., "Handling Qualities of a Large Civil Tiltrotor in Hover using Translational Rate Command," American Helicopter Society 68th Annual Forum, Fort Worth, TX, May 1-3, 2012.

6. Johnson, W., "Rotorcraft Aerodynamics Models for a Comprehensive Analysis," American Helicopter Society 54th Annual Forum, Washington D.C., May 20-22, 1998.

7. Rajagopalan, R. G., Baskaran, V., Hollingsworth, A., Lestari, A., Garrick, D., Solis, E., and Hagerty, B., "RotCFD - A Tool for Aerodynamic Interference of

Rotors: Validation and Capabilities," Future Vertical Lift Aircraft Design Conference, San Francisco, CA, January 18-20, 2012.

8. Gibertini, G., Auteri, F., Campanardi, G., Macchi, C., Zanotti, A., and Sabellini, A., "Wind-Tunnel Tests of a Tilt-Rotor Aircraft," *The Aeronautical Journal*, Vol. 115, No. 1167, May 2011.

9. Young, L. A., Yamauchi, G. K., and Rajagopalan, G., "Simulated Rotor Wake Interactions Resulting from Civil Tiltrotor Aircraft Operations Near Vertiport Terminals," 51st AIAA Aerospace Sciences Meeting including the New Horizons Forum and Aerospace Exposition, Grapevine, TX, January 7-10, 2013.

Table 1. Wind tunnel scale capacity and accuracy.

Scale	Range (lb)	Accuracy (lb)
LFL (Left Front Side)	0 to +1800	+/- 1.0
RFL (Right Front Side)	0 to +1800	+/- 1.0
RL (Rear Lift)	0 to +800	+/- 0.4
FSF (Front Side Force)	-2000 to +2000	+/- 2.0
RSF (Rear Side Force)	-2000 to +2000	+/- 2.0
Drag	-500 to +500	+/- 0.5

Table 2. LCTR and wind tunnel model parameters.

Parameter	Full-Scale LCTR	Wind Tunnel Model
Ratio to full-scale	1.0	0.06
Wing span (in)	1284	77.04
Inner wing span (in)	828	49.68
Inner wing sweep (deg)	-5.0	-5.0
Inner wing taper ratio	0.0	0.0
Inner wing incidence (deg)	+3.3	+3.3
Hub to hub (in)	924	55.44
Inner wing chord (in)	129	8.11 #
Nacelle length (in)	321	15.8 *
Nacelle diameter (approx.) (in)	88	4.8 *
Wing extension length (in)	180	10.8
Extension root incidence (deg)	+3.3	+3.3
Wing extension sweep (deg)	0.0	0.0
Wing extension taper ratio	0.41	0.41
Fuselage length (in)	1307	78.4
Fuselage diameter (in)	108	6.48

The wind tunnel model was based on the HETR wing geometry, which has a slightly smaller aspect ratio than the LCTR wing. This results in the model wing chord being slightly larger than 6% of the full-size LCTR wing chord.

* The wind tunnel model used nacelles based on the HETR tilt-rotor design, which are slightly smaller than the LCTR nacelles when scaled to 6% of full-size.



Figure 1: NASA LCTR design from Ref. 1.

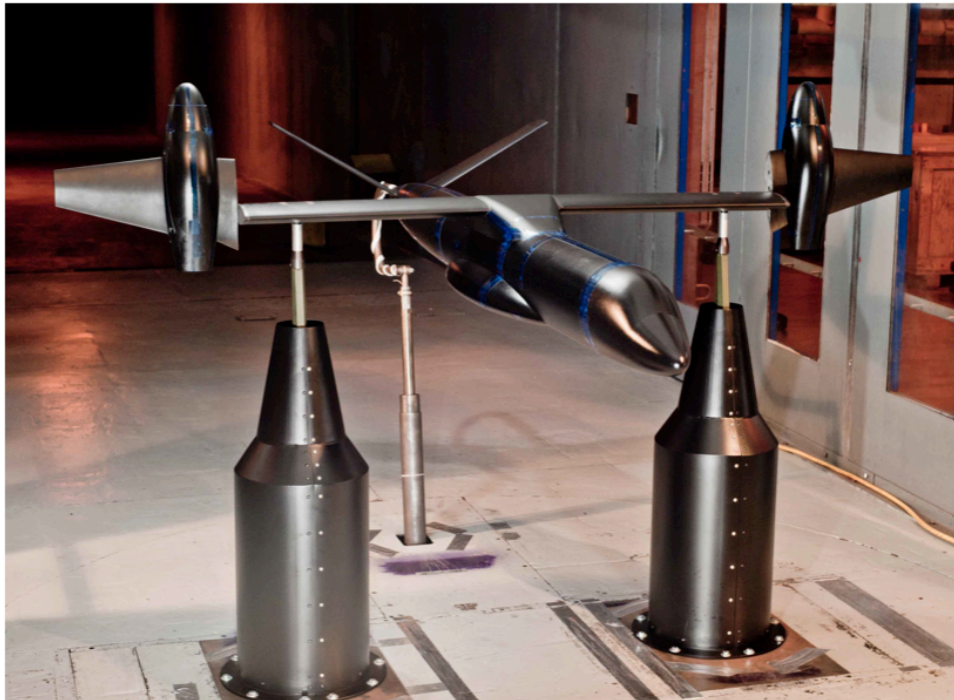


Figure 2: LCTR model in helicopter mode. The strut and fairing configurations shown were used for low-speed testing.



Figure 3: LCTR model in airplane mode. The strut and fairing configurations shown were used for high-speed testing.



Figure 4: Wing-only test configuration showing aerodynamic fairings for main wing struts.



Figure 5: Example SLS fuselage panel fitted to rib (left). LCTR model being assembled in the wind tunnel (right) showing 4-in square aluminum tube strongback with portions of the fuselage fitted forward and aft of the wing.

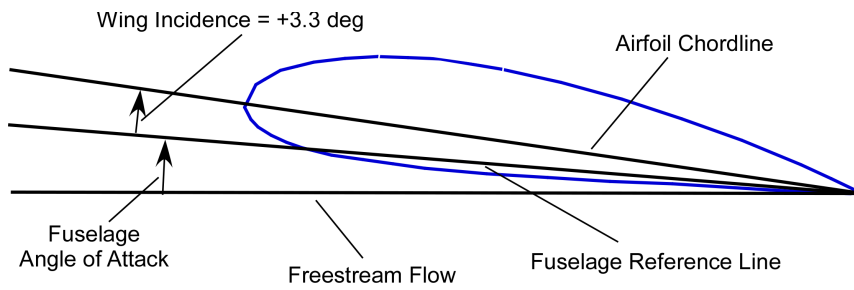


Figure 6: Wing and fuselage pitch angle definitions relative to the freestream flow. Note: A notional NACA4421 airfoil (21% maximum thickness) is shown for illustrative purposes only.

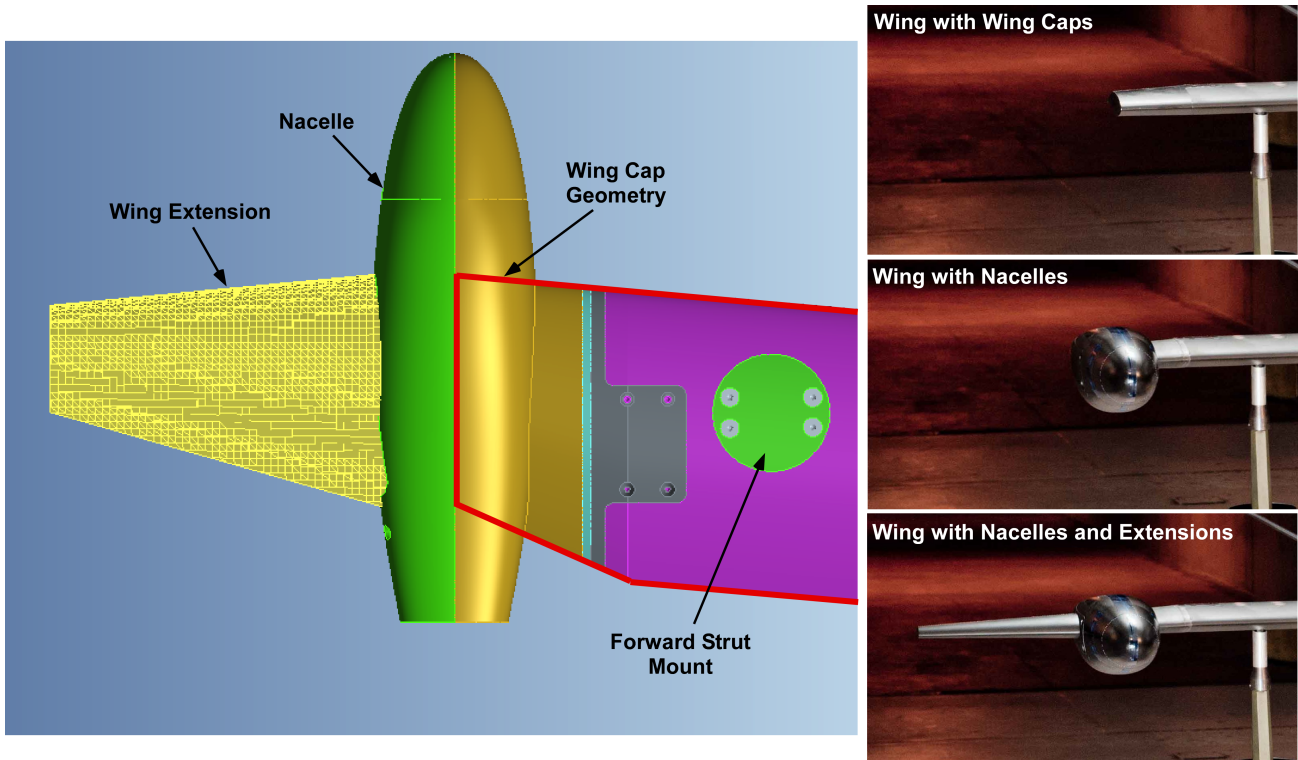


Figure 7: Graphic and photos of three different wing tip configurations tested. Red outline on left picture shows the wing geometry with a wing cap (nacelles and wing extensions removed). Nacelle configuration is with the wing extension removed.



Figure 8: Oil flow image with LCTR model in helicopter-mode configuration with nacelles aligned vertically.

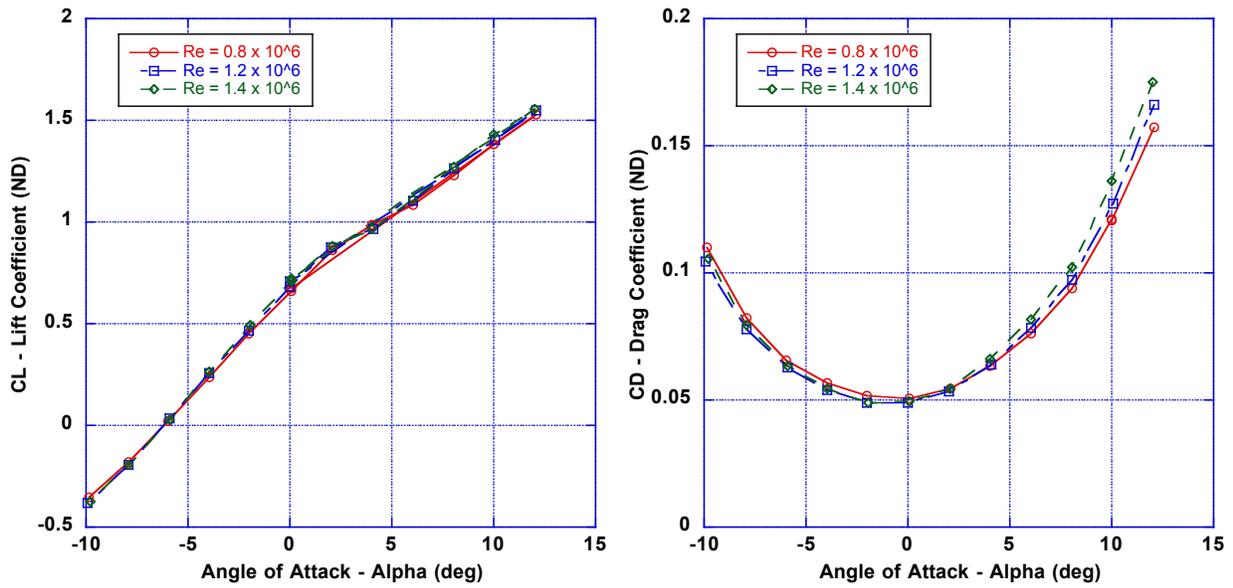
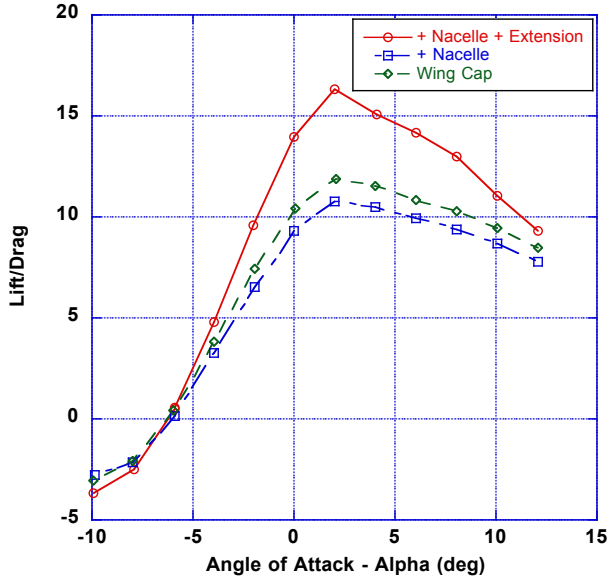
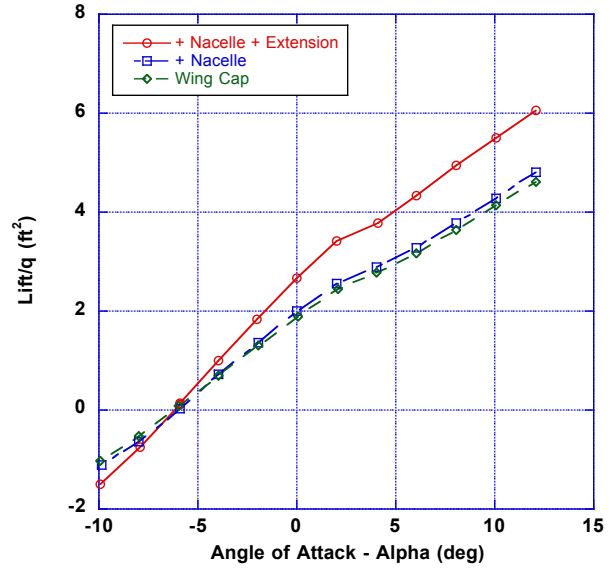


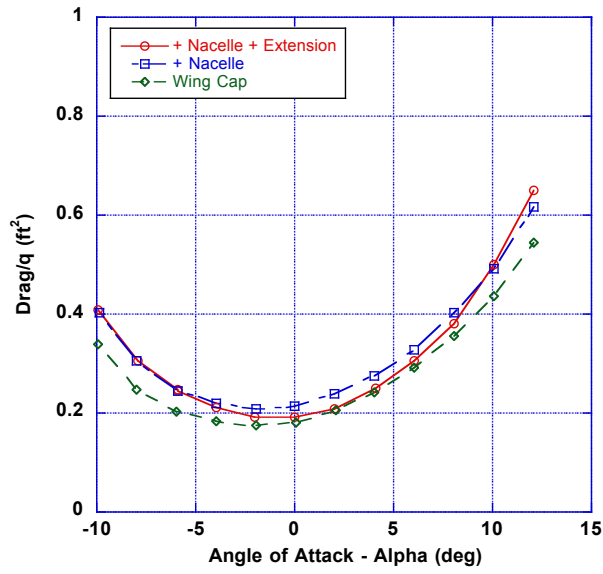
Figure 9: Effect of Reynolds number on lift and drag coefficient for LCTR model in airplane mode with the nacelles and wing extensions installed, $\beta = 0$ deg.



(a) Lift/Drag

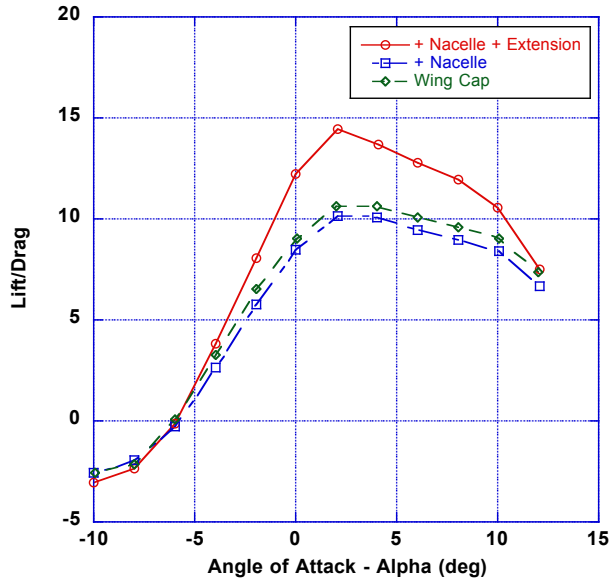


(b) Lift/q

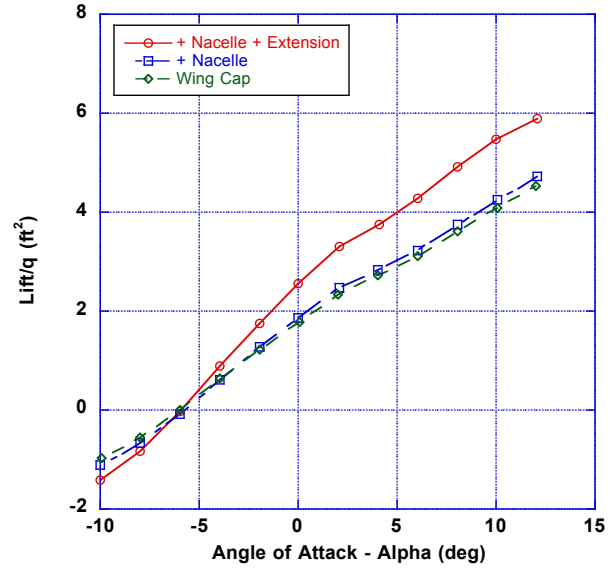


(c) Drag/q

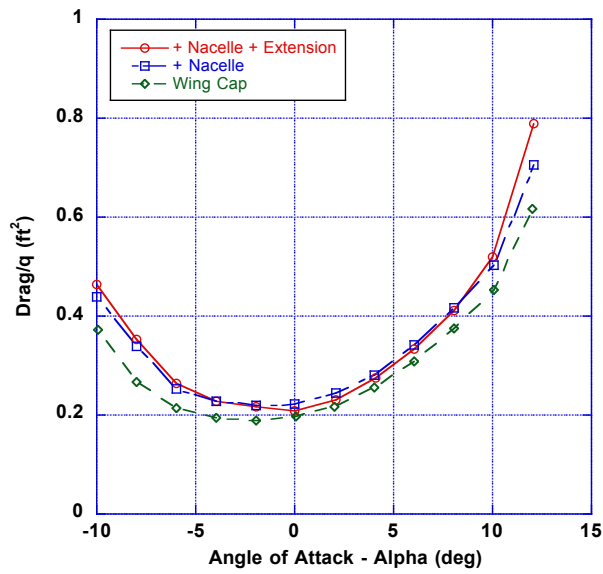
Figure 10: Effect of wing-tip configuration on LCTR airframe model aerodynamic loads for $\beta = 0$ deg., $V = \sim 168$ kt, $Re = 1.2 \times 10^6$.



(a) Lift/Drag

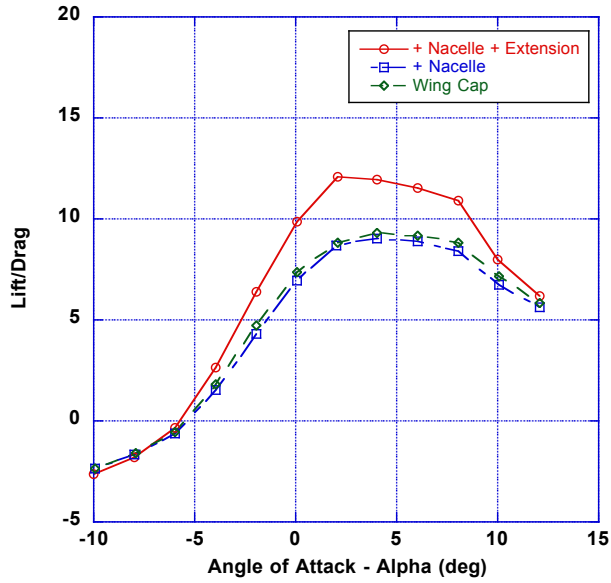


(b) Lift/q

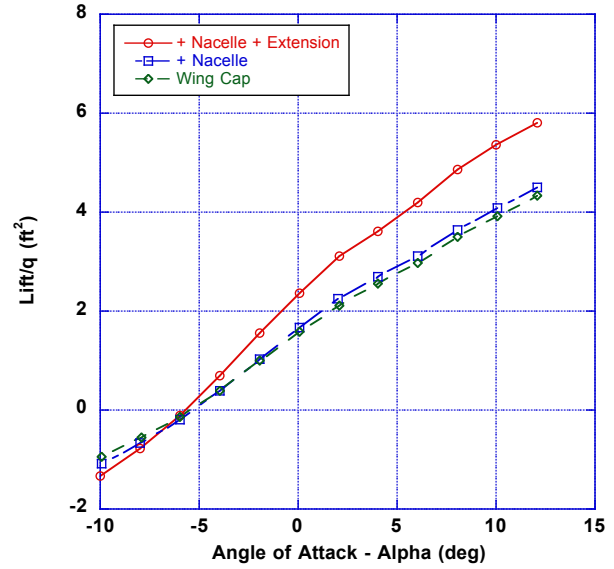


(c) Drag/q

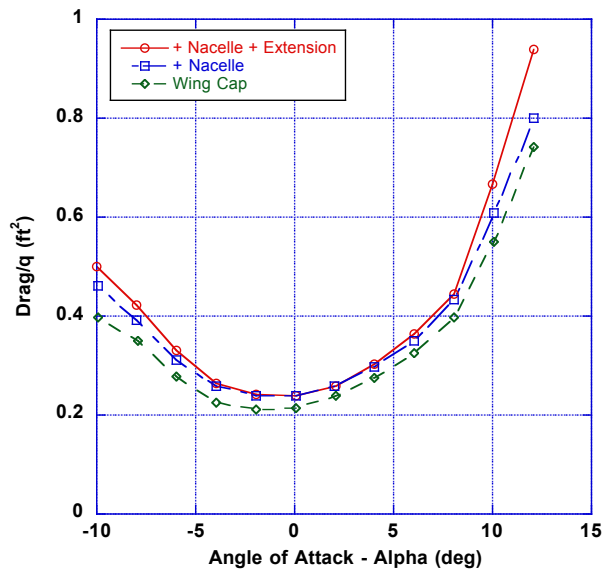
Figure 11: Effect of wing-tip configuration on LCTR airframe model aerodynamic loads for $\beta = +5$ deg., $V = \sim 168$ kt, $Re = 1.2 \times 10^6$.



(a) Lift/Drag

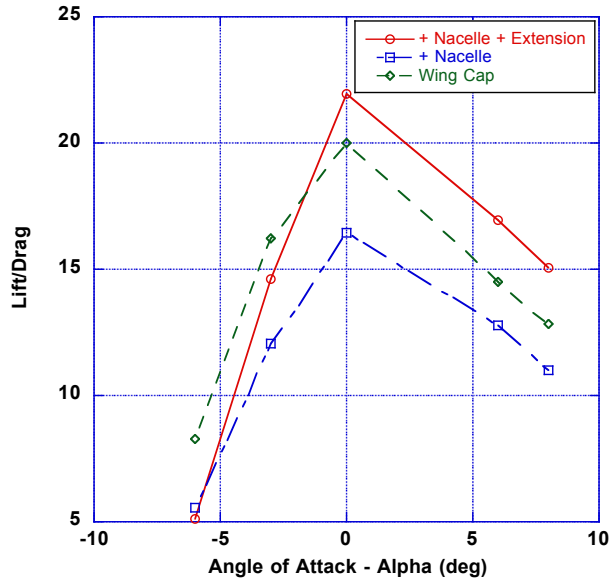


(b) Lift/q

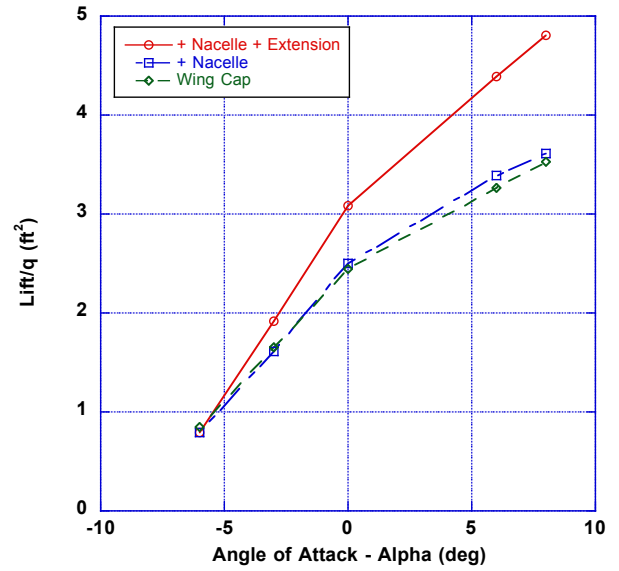


(c) Drag/q

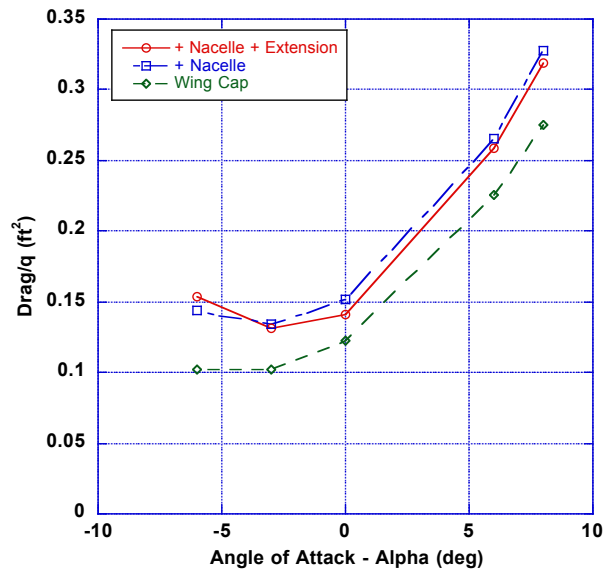
Figure 12: Effect of wing-tip configuration on LCTR airframe model aerodynamic loads for $\beta = +10$ deg., $V = \sim 168$ kt, $Re = 1.2 \times 10^6$.



(a) Lift/Drag



(b) Lift/q



(c) Drag/q

Figure 13: Effect of wing-tip configuration on wing-only configuration aerodynamic loads for $\beta = 0$ deg., $V = \sim 168$ kt, $Re = 1.2 \times 10^6$. The uncertainty in the drag measurement for the wing-only testing is of the order of 5-10%.